ELSEVIER

Polymer 42 (2001) 2479–2489

polymer

www.elsevier.nl/locate/polymer

Elemental mapping by ESI–TEM, during styrene emulsion polymerization

J.I. Amalvy[a,1], J.M. Asua[b], C.A.P. Leite[c], F. Galembeck[c,*]

[a]*CIDEPINT (Centro de Investigación y Desarrollo en Tecnología de Pinturas), Av. 52, entre 121 y 122 s/n, La Plata, Buenos Aires, Argentina*
[b]*Institute for Polymer Materials (POLYMAT) and Grupo de Ingeniería Química, Departamento de Química Aplicada, Facultad de Ciencias Químicas, Universidad del País Vasco, Apdo. 1072, 20080 San Sebastián, Spain*
[c]*Department of Chemistry, Instituto de Química, Universidade Estadual de Campinas, Caixa Postal 6154, 13083-970, Campinas, SP, Brazil*

Received 7 January 2000; received in revised form 2 May 2000; accepted 9 June 2000

Abstract

The elemental distribution in latex particles during the ab-initio and seeded emulsion polymerization of styrene was studied by electron spectroscopy imaging, in an analytical transmission electron microscope. Surface anchoring effect, chain migration and the extent of burying of the sulfate groups from the initiator were investigated by comparing the distributions of the different elements.

Keywords: Latex particles; Seeded emulsion polymerization; Styrene

1. Introduction

The control of latex particle morphology is essential in the making of a functional product. Core–shell morphology is now routinely used in the synthesis of latex for paints, where two or more monomers are copolymerized. For example, a core of a glassy polymer imparts gloss and hardness to the latex film, and a rubbery shell enables the latex particle to form a uniform surface coating. Well-designed intraparticle inhomogeneity in emulsion polymerization is now achieved and different types of morphologies (e.g. core–shell, acorn-shaped) are well established in emulsion copolymerization [1–5].

It has also been claimed that core–shell inhomogeneities might arise in an emulsion homopolymerization, but evidence for this characteristic morphology is less conclusive [6–11].

Based on kinetic analysis of experimental data, Williams et al. [6,7] proposed a non-uniform "core–shell polymerization" in styrene latexes. According to these authors, the growing particle consists of a polymer-rich core and a monomer-rich shell. Williams et al. [6,7] also provided morphological evidence to support their theory, as they used butadiene to produce a copolymer with styrene and the unsaturated butadiene units were stained with osmium tetroxide. An ultrathin section taken through the center of the particle showed a doughnut shape. Chang and Chen [12] proposed a diffusion-controlled core–shell model, assuming a nearly dry core (without monomer in the inner part of the particle) that yielded a non-uniform morphology to explain the experimental results. However, no direct evidence was provided to support this theory.

Particle inhomogeneity may also arise from the surface anchoring effect [13]. Water-soluble initiators (e.g. potassium, sodium or ammonium persulfates) are most commonly used in emulsion polymerization. The thermal decomposition of the persulfate ion leads to the formation of sulfate ion-radicals ($S_2O_8^{2-} \rightarrow 2SO_4^{\cdot -}$). These react with monomer molecules to form the oligomeric radicals, initially soluble in the aqueous phase. These water-soluble oligomeric sulfate ion radicals add more monomer units to the chain until they become surface active and adsorb at the interface of the monomer swollen polymer particles. The radical ends are then expected to be oriented towards the hydrophobic monomer–polymer phase, and the sulfate groups are oriented towards the aqueous phase.

Chern and Poehlein [14] showed by simulation that surface anchoring effect yields a non-uniform distribution of radicals in the polymer particle, the concentration near the surface being higher than in the interior. This non-uniform distribution of radicals promotes the formation of core–shell morphologies [15].

* Corresponding author. Tel.: +55-19-289-3118; fax: +55-19-788-3023.
E-mail address: fernagal@iqm.unicamp.br (F. Galembeck).
[1] Member of Research Career of CIC, Buenos Aires, Argentina.

0032-3861/01/$ - see front matter
PII: S0032-3861(00)00433-X

Analytical methods have been developed to measure the sulfate and other surface groups in polystyrene latex, such as ESCA [16], dye-partition methods [17], IR spectroscopy [16] and conductimetric titration [13,18]. Vanderhoff [13] found experimental evidence for the surface anchoring of hydrophilic sulfate chain-ends on the particle, by conductimetric titration. Kamel et al. [18] found that polystyrene latex contains also buried sulfate groups, which is easy to understand considering that concentrating all the sulfate groups at the particle surface would force polymer chains into stretching, thus departing from the relaxed, most probable chain conformations.

Recently, Cardoso et al. [19] introduced the technique of electron spectroscopy imaging (ESI) in the transmission electron microscope (TEM) to study the morphology of S/HEMA latex. This technique allows to determine the elemental distribution in latex particles and will be used in the present work to assess the importance of the surface anchoring effect and the chain migration in the polymer particles for both the ab-initio batch and the seeded semicontinuous emulsion polymerization of styrene.

2. Experimental

The following chemicals were used as received. Styrene (S) and Aerosol MA 80 (Cyanamid) (sodium dioctyl sulfosuccinate) were technical grade. Potassium persulfate (KPS) and sodium bicarbonate (SBC) were of analytical grade. Water was deionized and distilled (DDW).

Batch emulsion polymerization of styrene was carried out using the following amounts of reagents: water, 626.5 g; styrene, 267.0 g; sodium bicarbonate, 1 g, surfactant Aerosol MA 80 (cyanamid), 11.45 and potassium persulfate 1.005 g. The polymerization was carried out at 90°C, in a 1000 ml glass reactor fitted with condenser, thermocouple, stirrer and nitrogen inlet. Almost complete conversion was achieved in about 1 h. The system was held at 90°C for 16 h at 250 rpm to destroy unused initiator. A 31 wt% solids content latex was obtained. Samples were withdrawn during the reaction, the polymerization was short-stopped with a 1% aqueous hydroquinone solution and conversion and particle size determined as detailed below.

The average internal viscosity of the polymer particles is lower for the batch process than for the semicontinuous process. Therefore, the polymer chains are expected to be more mobile in the batch emulsion polymerization. This might allow the sulfate groups from the initiator to remain at the surface of the particle avoiding burying during the particle growth. Consequently, in the final particles, the sulfate groups might be concentrated near the surface of the particle. On the other hand, in the semicontinuous process, the high interval viscosity of the polymer particles restrict the movement of the polymer chains, and these will likely stay in the place where they were formed, leading to a significant burying of the sulfate end groups. Therefore, a relatively uniform distribution of sulfate groups in the final polymer particle could be expected. Seed semicontinuous emulsion polymerization was carried out at 70°C, using the latex obtained in the batch process as a seed. The initial charge contained 100.5 g of seed latex 300 g of DDW, the initiator and the buffer. 60 g of styrene were fed at 0.3 g/min. This amount of styrene was calculated in order to increase the particle size to about one and half that of the seed particles. Final total solids content was about 18 wt%.

Serum replacement [20] was used to separate the serum from the latex particles flushing distilled water through a filtration cell (UHP-76 of MicroFiltration Systems) in a continuous mode.

Samples taken during the reactions were analyzed using TEM and electron energy-loss spectroscopy, in a Zeiss CEM902 microscope. The surface charge density was determined by conductimetric titration using NaOH as titrant.

Particle size was determined by light scattering (LS) with a Coulter N4Plus apparatus. This technique gives an intensity weighted average particle size, $d_{\text{intavg}} = \sum(n_i I_i d_i)/\sum(n_i I_i)$, where I_i is the intensity of light scattered from particles of diameter d_i and n_i the number of such a particles. This value is close to the *z*-average particle size ($d_z = \sum(n_i d_i^7)/\sum(n_i d_i^6)$).

Samples for microscopy were prepared by diluting the washed particles with double distilled water, and applying one drop of the latex dispersion to carbon-coated parlodion films supported in 400 mesh copper grids (Ted Pella). Other experimental details regarding TEM are presented elsewhere [19]. To make sure that the contrast observed in the elemental maps refers to the whole particle, not just to a thin particle section, we first observed each sample with monochromatic electrons, at zero energy-loss as well as at 20–50 eV energy-loss. This causes a complete contrast inversion in every case reported in this paper, showing that the electrons are actually sampling the whole particle thickness, even at their centers. This is actually expected, considering that the diameter of the larger particles is in the same order of magnitude of the electron mean free path, for electron inelastic collisions within polystyrene [21].

To obtain more information on the relative intensity of elements distribution between particles from different samples, we prepared a mixed sample consisting of particles of very different sizes, where the visual identification of each component was possible. Densitometer double line profiling of a given width (10% of particle size, for noise averaging) was performed in a PC, using the SigmaPlot software. The line profiling was performed throughout the particles, giving a three-dimensional (3D) elemental distribution of pixel gray level as a function of the *x–y* plane coordinates.

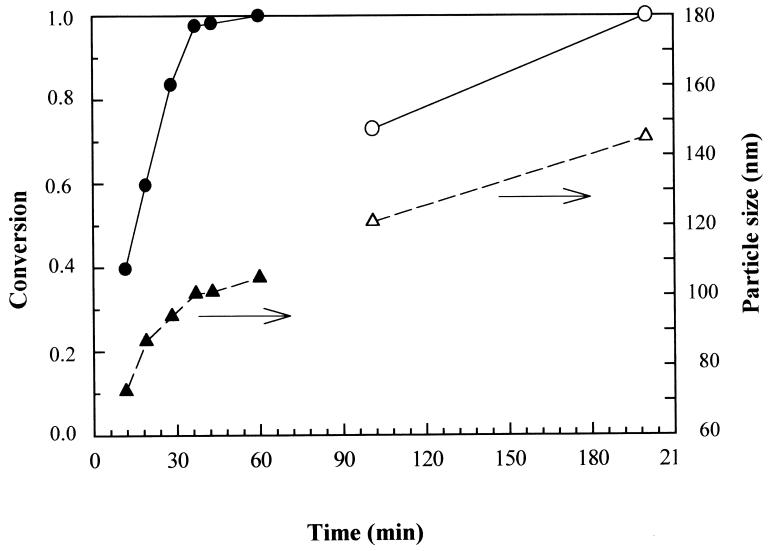

Fig. 1. Conversion (●) and particle size (▲) evolution during the synthesis of the seed latex. Conversion (○) and particle (△) size evolution for the seeded semicontinuous emulsion polymerization.

3. Results and discussion

3.1. Conversion and particle size evolution

Samples withdrawn from the polymerization reactor were identified as S1, S2…S6 (for the seed formation step) and E1, E2 (for the seeded polymerization step). Fig. 1 shows the conversion and particle size evolution of the styrene emulsion polymerization, which follow the expected pattern. Table 1 gives latex data for the various samples collected during polymerization. Particle size on this table corresponds to unswollen particles.

Calculations using the data in Table 1 show that the number of polymer particles did not vary during the semicontinuous process.

3.2. Element distribution within the particles

Element distribution is presented in (Figs. 2–8) — the micrographs in Figs. 2, 4, 6 and 8, and in the 3D plots, in Figs. 3, 5 and 7. The micrographs are arranged in plates, displaying a standard bright-field image, together with element maps for all major latex constituent elements: C, K (from the counter-ions), S (from the initiator residues and surfactant) and O (from the initiator, surfactant and water molecules trapped in the particles).

In the bright-field picture, an image pixel appears darker when it is covered with a thicker particle section, or with electronically denser material, through which electron transmission is impaired. Since the field illumination is not uniform, the centers of these images appear brighter than their periphery. In any given picture, the larger particles are darker than the smaller ones, due to lower electron transmission; for the same token, particle borders and interparticle necks appear clearer than particle centers.

In the elemental maps, any pixel appears brighter whenever it is covered with a greater amount of a given element. This may be due to two factors: first, the sample thickness at this pixel may be higher; second, the element concentration is the column of material covering this pixel is higher. Consequently, the contrast in the elemental maps reveals point-to-point particle composition variations, as well as composition differences from one to another particle. This

Table 1
Data on samples taken during the polymerization experiments

Sample	Time (min)	Conversion (%)	Particle diameter (nm)	Surface charge ($\mu C/cm^2$)
Ab-initio emulsion polymerization				
S1	12	39.7	73	Not detectable
S2	19	59.7	87	Not available
S3	28	83.9	94	Not available
S5	43	98.4	101	Not available
S6	24 h	99.9	105	~1
Seeded emulsion polymerization				
E1	101	73 (total)	121	Not detectable
E2	200	98.8	145	~1

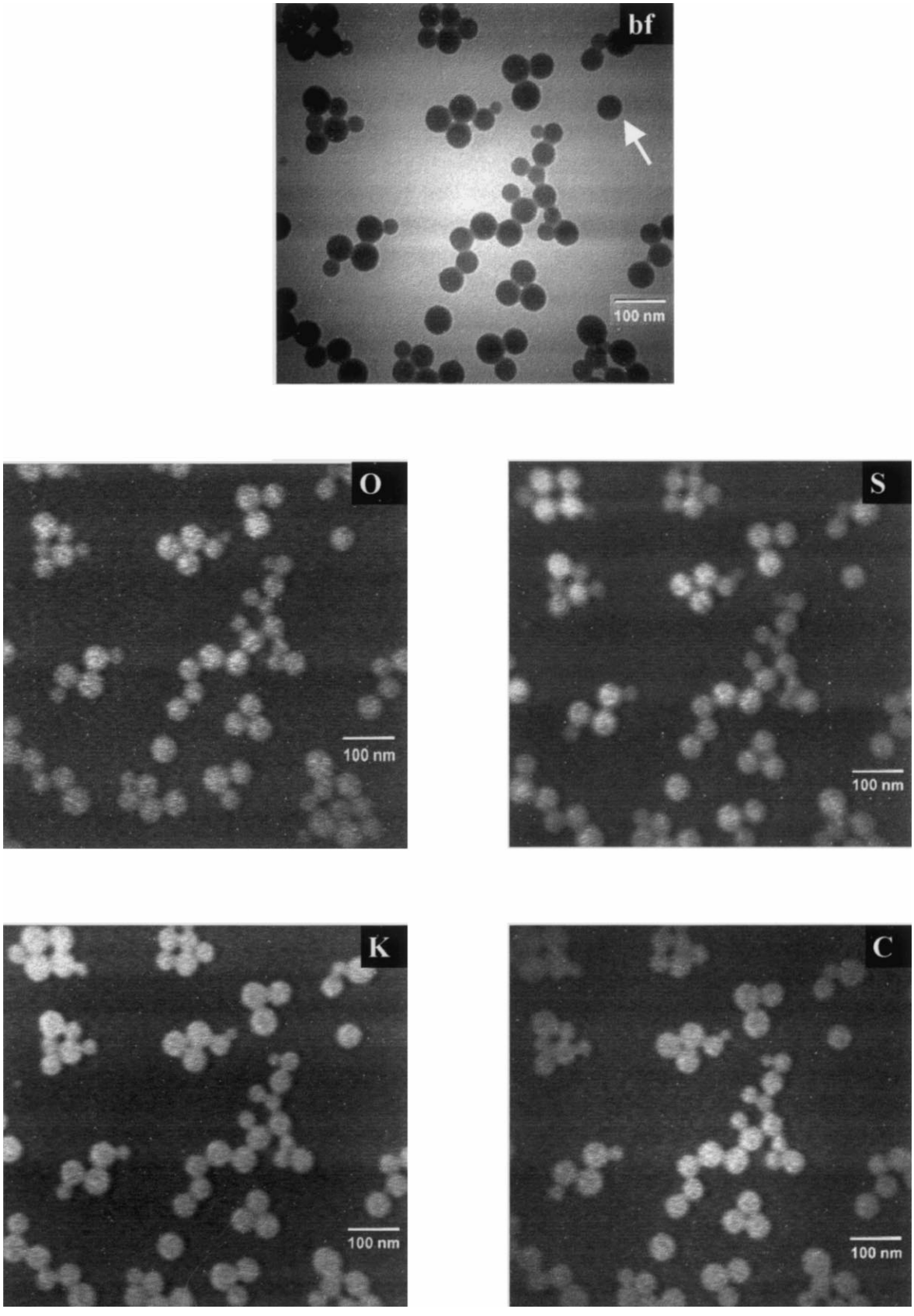

Fig. 2. Bright-field image and elemental maps of S1 sample.

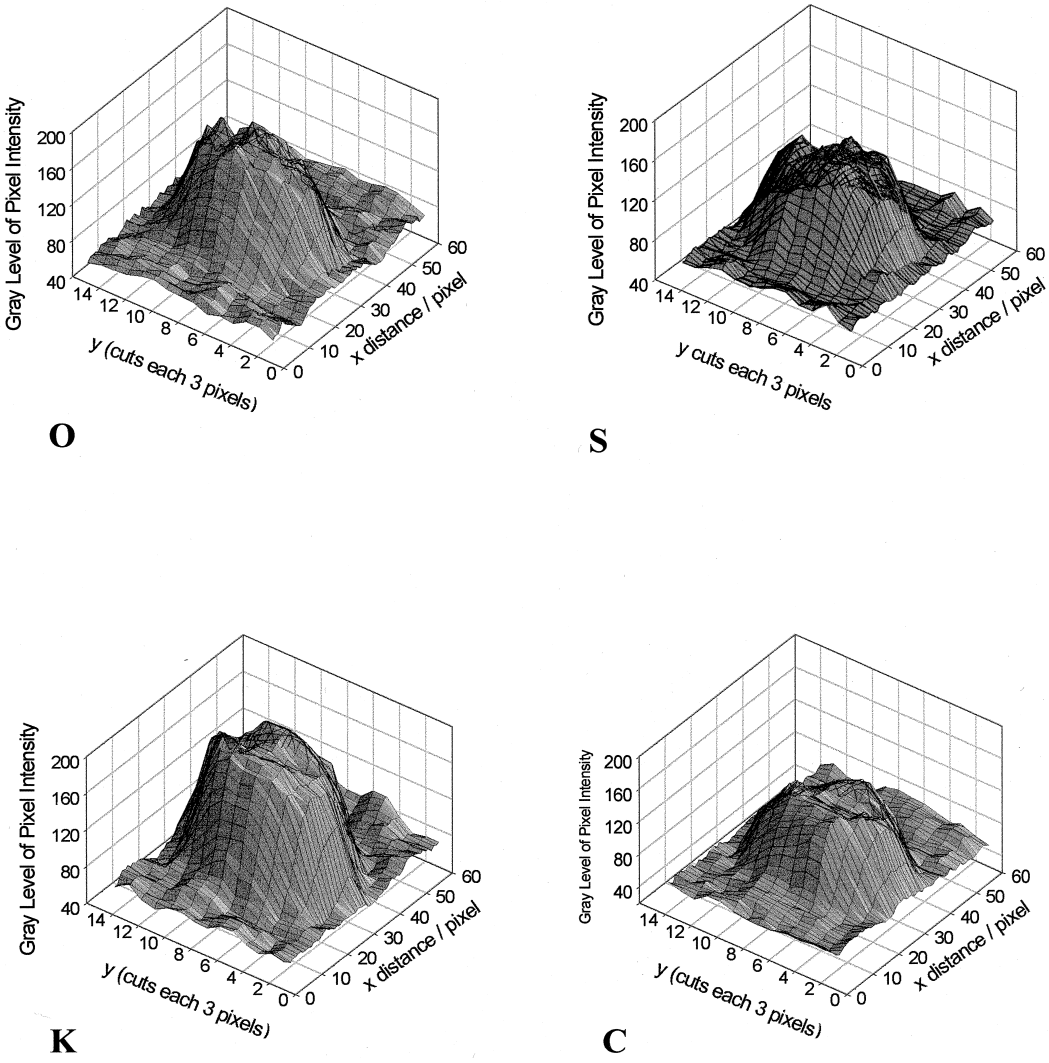

Fig. 3. 3D gray level intensity plots for S1, obtained from the particle indicated with an arrow in Fig. 2.

is reflected in the 3D plots, in which the gray level is represented in the vertical axis as a function of pixel position, and it is thus correlated to the amount of the mapped element above a given (x,y) point in the respective micrograph.

3.3. Sample S1

Figs. 7 and 3 present the bright-field image and elemental maps of the polymer particles (S1) sampled from the batch reactor at a conversion of 0.397. The C map presents some local maxima within the particles, but without following a definite pattern. Adjacent particles display similar intensities, as expected since this is their main constituent element. The carbon 3D plot in Fig. 3 is better described as a flattened dome rather than as a pointed dome corresponding to a uniform distribution of carbon through a spherical particle. As carbon is the main component of the polymer particle, it is likely well distributed through the particle. This means that the particles are flattened in the sample holder. The sulfur 3D plot does not present any significant variation with respect to the shape of the carbon 3D plot. This means that sulfur is also rather uniformly distributed in the polymer particle. On the other hand, in the S distribution map, there is strong contrast between adjacent particles of the same size, evidencing a heterogeneous distribution of this element between particles. The larger particles also display internal bright spots, which are assigned to the accumulation of S in some domains. On the other hand, the smaller particles display a uniform gray level, without any evidence for local S accumulation within each particle. Larger particles are brighter because they have much more initiator residues. The oxygen atom distribution follows the same pattern as sulfur, but the bright spots in the larger particles are more marked than in the S case. This mismatch between sulfur and oxygen contrast shows that oxygen is not solely associated to sulfur, in the persulfate initiator residues or in the trapped surfactant molecules, and it may be also assigned to two factors: the first is the presence of residual solvating water, within some domains accumulating significant local concentrations of the polar

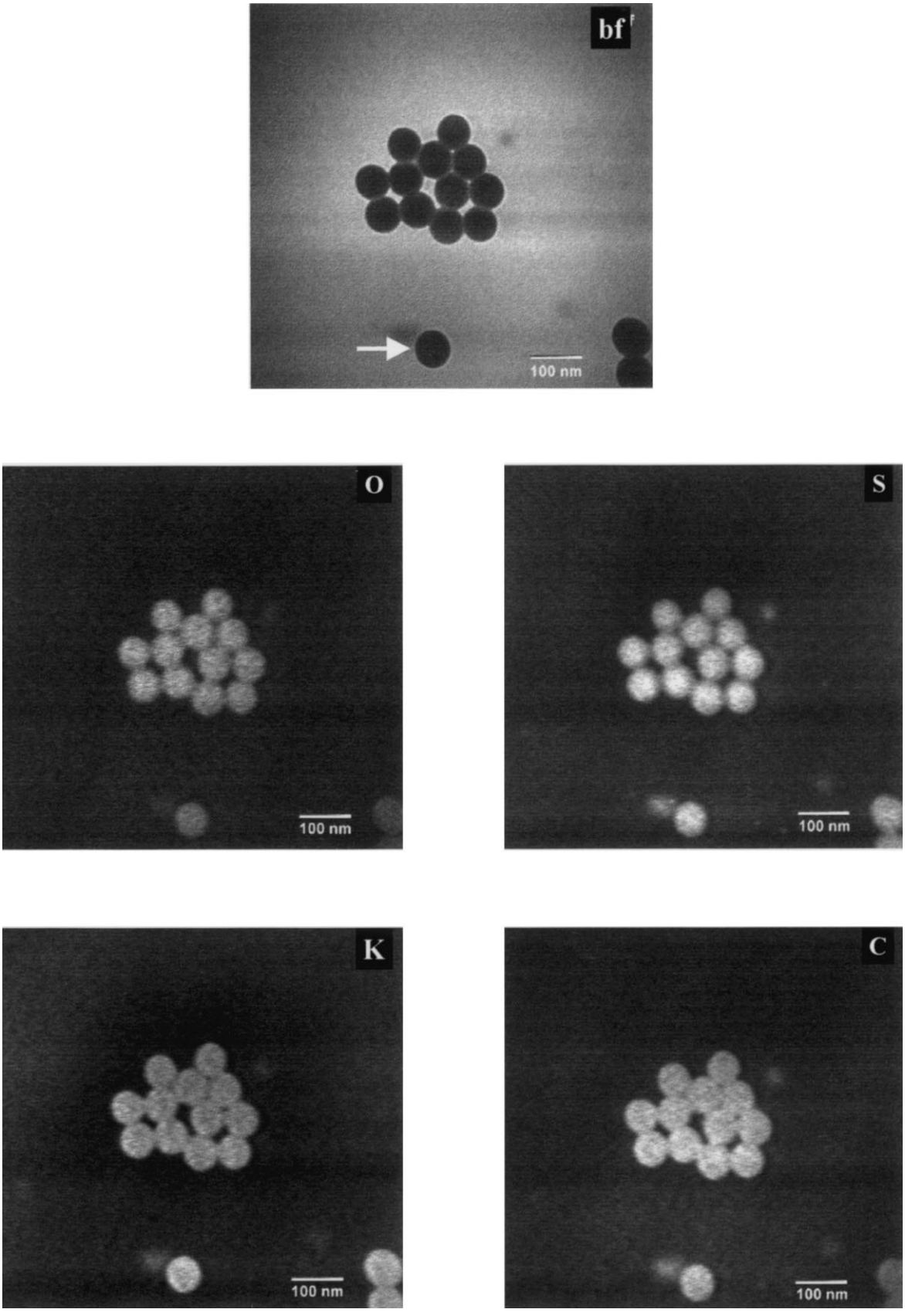

Fig. 4. Bright-field image and elemental maps of S3 sample.

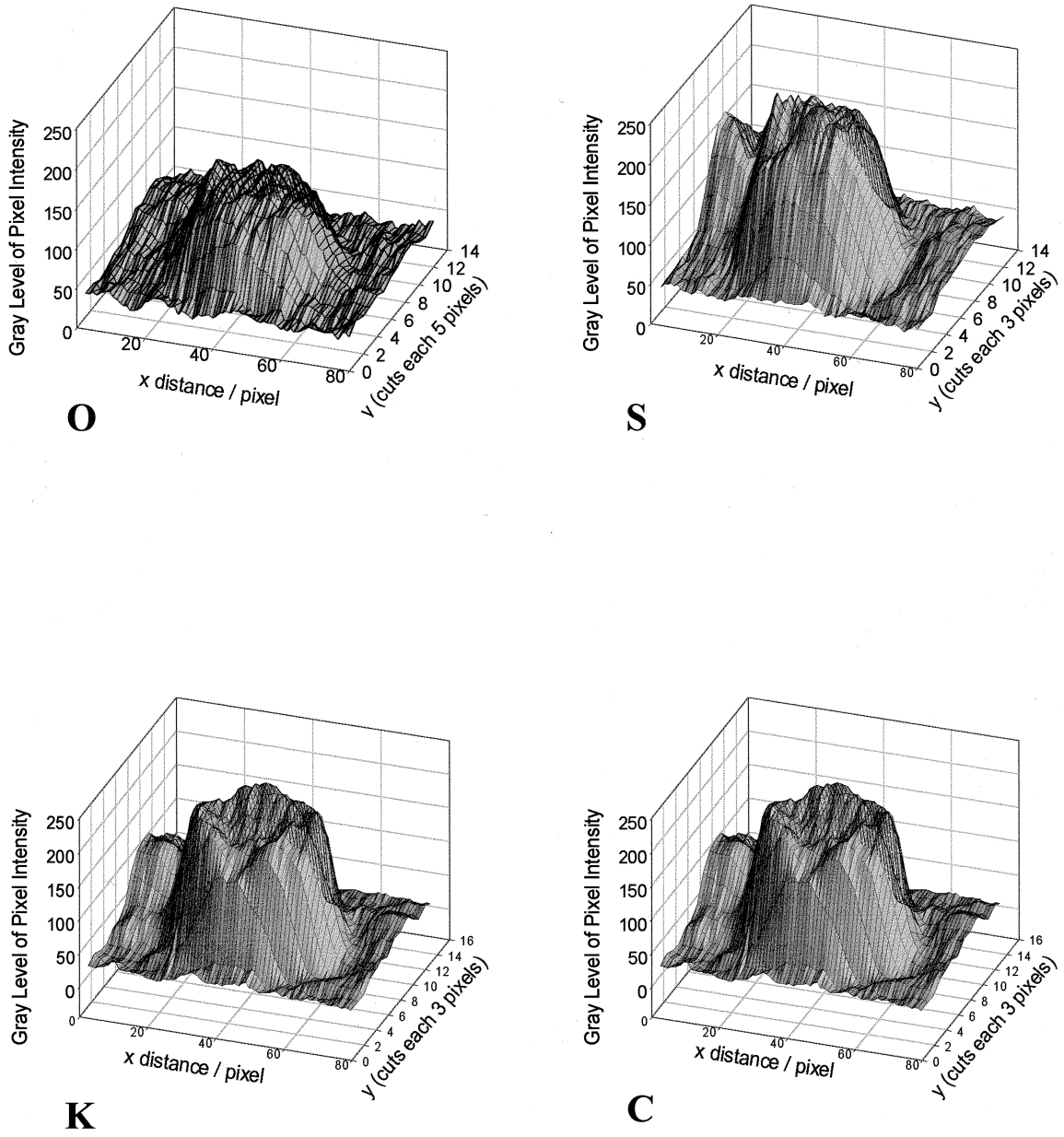

Fig. 5. 3D gray level intensity plots for S3, obtained from the particle indicated with an arrow in Fig. 4.

(sulfate, sulfosuccinate and potassium) groups; second, the hydrolysis of part of the sulfate-terminated chains during the polymerization leaves hydroxo groups at chain-ends, which cluster together with the other polar groups. Finally, the potassium distribution is more uniform than S distribution, across the particles as well as from one to another particle. This observation does not support a widespread assumption, which is the segregation of ionic species to the particle surface, in PS latex. On the other hand, the mismatch between K and S images, which is particularly high in the smaller particles, is an evidence for a competition among K^+ and the other (Na^+, H^+) counter-cations present in the serum.

3.4. Sample S3

Elemental distribution maps for sample S3 (batch process, 83.9% conversion) are given in Fig. 4 and the corresponding 3D plots are in Fig. 5. The S3 particles in the field depicted are more uniform in size than the S1 particles, but we can also see some cloudy, poorly defined particles with a low contrast in the bright-field image, but a strong contrast in the elemental maps. Observing the elemental distribution maps in Fig. 4, we notice a distinction between S and O maps, as compared to K and C maps: in the former, the frontiers among particles are better seen than in the latter. The amounts of initiator and surfactant residues are thus larger within the particles than at the particle

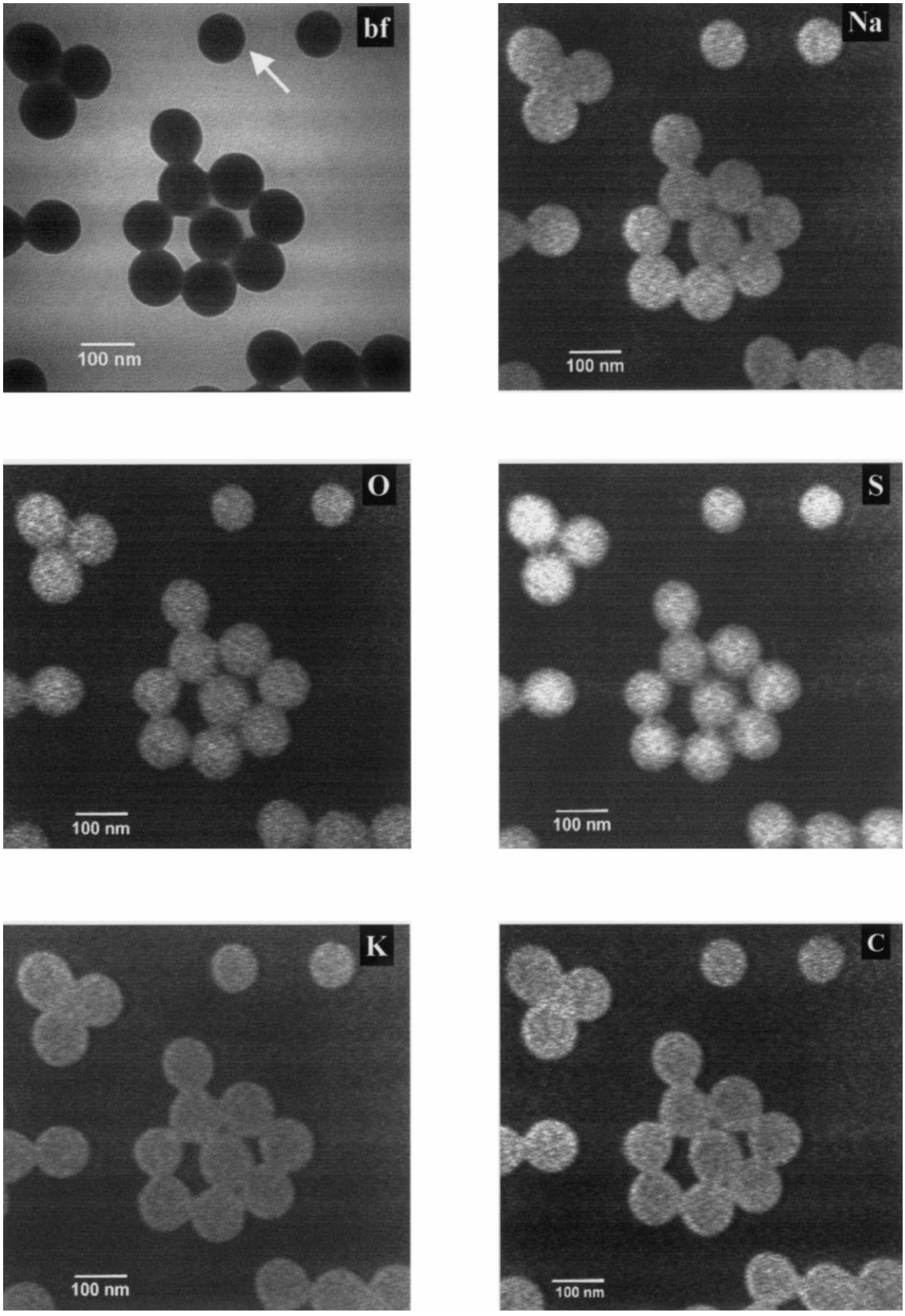

Fig. 6. Bright-field image and elemental maps of E2 sample.

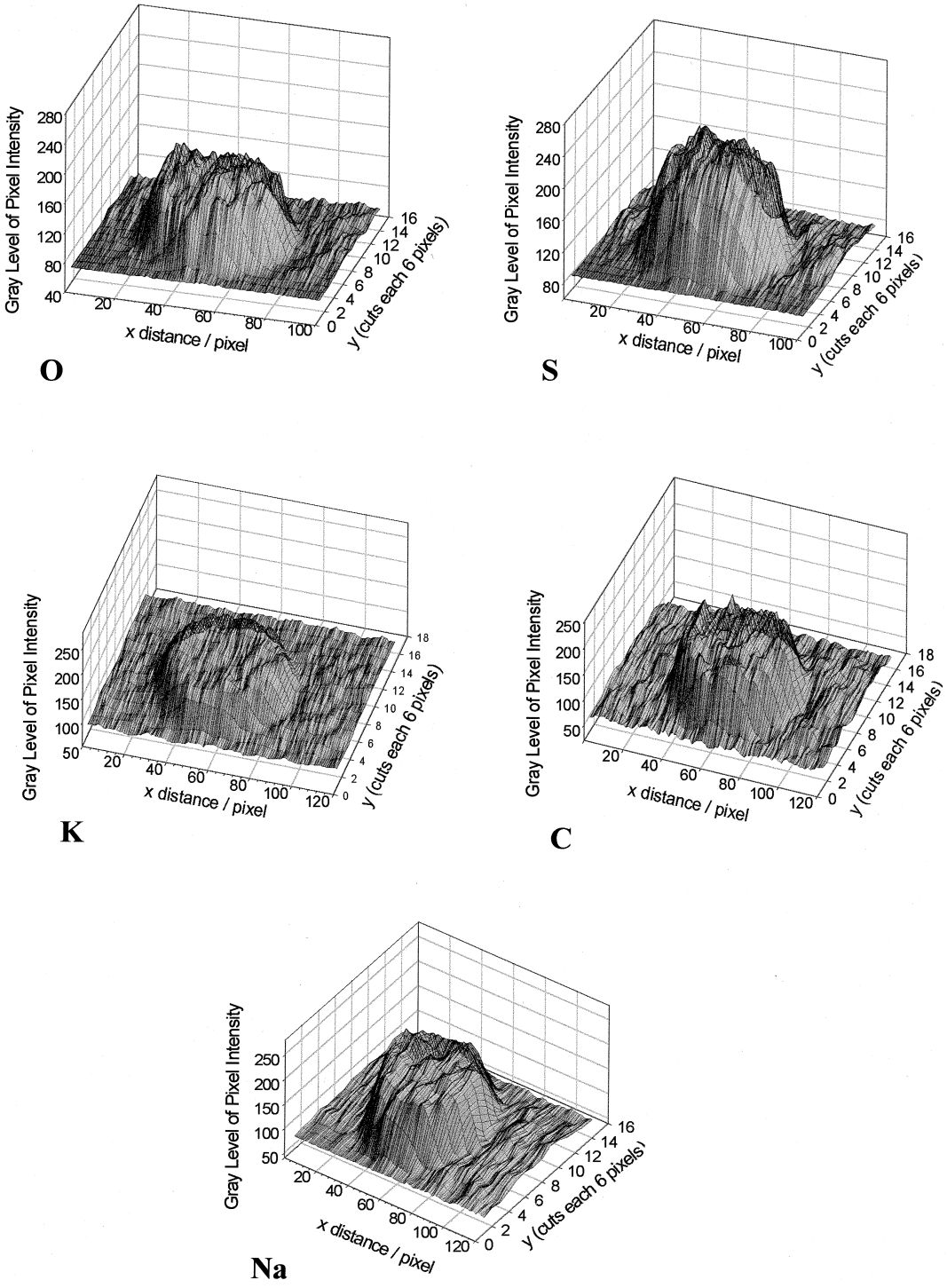

Fig. 7. 3D gray level intensity plots for E2, obtained from the particle indicated with an arrow in Fig. 6.

borders, following the same pattern previously identified in a copolymer latex [19]. Potassium is distributed throughout the S3 particles, as in the case of S1 sample. However, there is also some definite K distribution maxima, closer to the particle outer shells. The C distribution differs from S1, following well-defined peripheral maxima. This may be understood considering that the dry particles in the microscope sample holder are flattened, which is actually seen in the bright-field picture, where the gray level is rather uniform, in the central part. A depression is seen in the center of the 3D carbon map plot in Fig. 5, which may be due to particle flattening as well as the following three other factors: (i) a higher free-volume within these particles, due to the presence of swelling monomer residues; (ii) apolar,

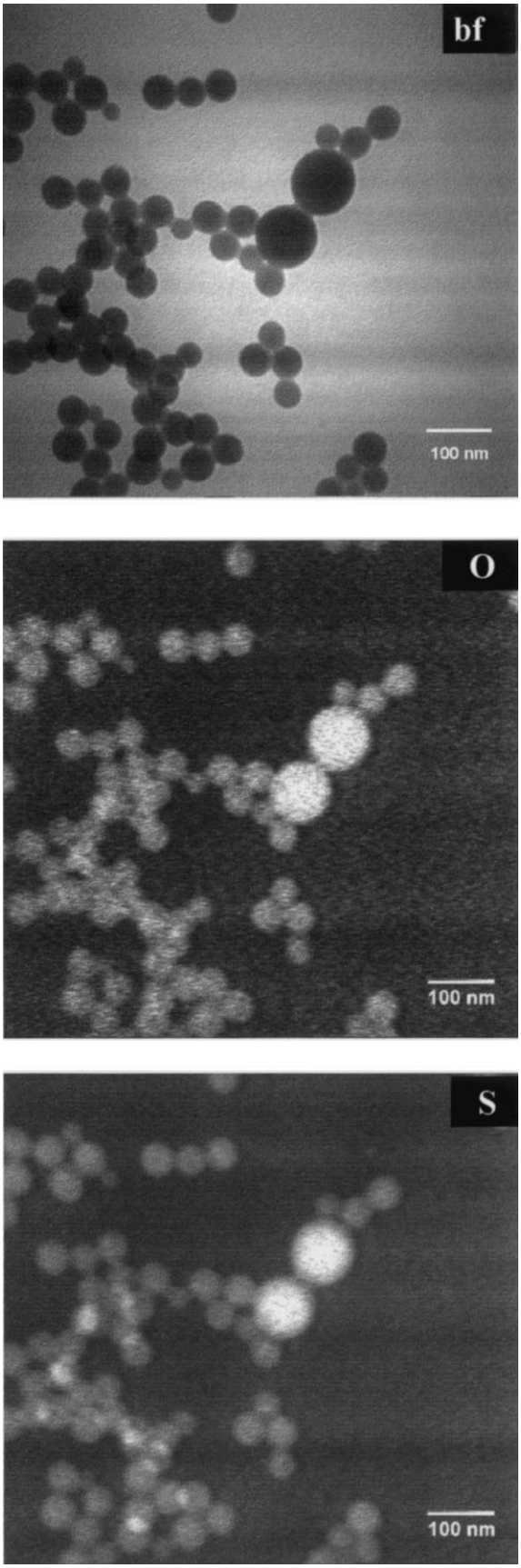

Fig. 8. Bright-field image and elemental maps of S1 + E2 mixed sample.

low surface tension chain migration to the particle surface, during sample drying and preparation for microscopy and (iii) an increase in polymer density from the particle center to the particle surface, arising from differences in the degree of chain branching and configuration. Figs. 6 and 7 present the elemental distribution maps and the corresponding 3D plots for polymer particles sampled at the end of the semicontinuous polymerization. This polymerization was carried out in an attempt to investigate the effect of particle viscosity on sulfate group distribution. The carbon 3D plot suggests particle flattening. Sulfur 3D plot also looks like a flattened dome, without much difference with respect the 3D plots for the batch products, namely, no evidence of an effect of particle viscosity on sulfur distribution was found.

3.5. Sodium and potassium distribution, in sample E2

Sodium distribution maps were also obtained in this case. Na follows a distribution pattern less uniform than potassium, evidenced by the sharp brighter spots within the particles, and in both cases there is an increase of intensity in domains at the peripheral zone of particles.

The distinction between Na and K maps is assigned to the difference in their hydrated radii. It was suggested by Su et al. [22] using titration and dielectric spectroscopy, that the degree of counterion binding to the particle is a function of the hydrated ion size. Potassium has the larger radius in an anhydrous crystal lattice, but its hydrated ionic radius is lower than that of sodium, for which reason the partitioning of the two ions between media of different polarities should not be identical.

3.6. Mixed sample S1 + E2

Particles from these two samples were mixed, and examined together to allow for a direct comparison, within the same fields (Fig. 8). The brighter regions correspond to larger E2 particles, or to superimposed S1 particles. The smoother distribution of S, as compared to O, is confirmed here.

3.7. Conductimetric titration

Some samples were analyzed with respect to the surface charge, but no differences between final samples of both processes were detected, indicating that sulfate groups were buried inside the particles. This observation agrees with the elemental maps described in this work, and with previous results in the literature [23,24].

4. Conclusions

The elemental distribution in latex particles obtained by both ab-initio batch emulsion polymerization and semicontinuous seeded emulsion polymerization was studied by ESI, in an analytical TEM. The carbon 3D plot suggests that polymer particles become flattened in the sample holder.

The sulfur 3D plot also presents a flattened dome shape. For a spherical particle, this shape would be a proof of a preferential accumulation of sulfur near the surface of the polymer particle. However, for a flattened particle this conclusion is not straightforward. A comparison of the shapes of the carbon and sulfur 3D plots suggests that sulfur is uniformly distributed through the polymer particle, namely, that polymer chains remain at the place where they were formed and the sulfate group from initiator residues are not able to stay near the surface of the polymer particle avoiding burying. This conclusion applies to both batch and semicontinuous process, i.e. sulfate groups burying is not affected by particle viscosity. No conclusive proof for surface anchoring effect was found.

Acknowledgements

Part of this work was carried out during a postdoctoral fellowship of J.I.A. supported by AECI-UPV and the Basque Government. J.I.A. also acknowledges the support as visiting professor from Instituto de Química-UNICAMP (Brasil), (FAPESP Project no. 95/3636-3). FG acknowledges the support of CNPq, Fapesp and Pronex/Finep/MCT.

References

[1] Okubo M. Makromol Chem Macromol Symp 1990;35/36:307.
[2] Shen S, El-Aasser MS, Dimonie VL, Vanderhoff JM, Sudol ED. J Polym Sci, Polym Chem Ed 1991;29:857.
[3] González-Ortiz LJ, Asua JM. Macromolecules 1995;28:3135.
[4] González-Ortiz LJ, Asua JM. Macromolecules 1996;29:383.
[5] González-Ortiz LJ, Asua JM. Macromolecules 1996;29:4520.
[6] Grancio MR, Williams DJ. J Polym Sci A1 1970;8:2617.
[7] Keusch P, Williams DJ. J Polym Sci, Polym Chem Ed 1973;11:143.
[8] Keusch P, Graff RA, Williams DJ. Macromolecules 1978;7:304.
[9] Linné P, Klein A, Sperling LH, Wignall GD. Macromol Sci Phys 1988;B27(2/3):181.
[10] Lau W, Westmoreland W, Novak RW. Macromolecules 1987;20:457.
[11] Westmoreland W, Lau W. Macromolecules 1989;22:496.
[12] Chang HS, Chen SA. J Polym Sci, Polym Chem Ed 1988;26:1207.
[13] Vanderhoff JM. Characterization of metal and polymer surfaces. New York: Plenum, 1977 (p. 365).
[14] Chern CS, Poehlein GW. J Polym Sci, Polym Chem Ed 1987;25:617.
[15] de la Cal JC, Urzay R, Zamora A, Forcada J, Asua JM. J Polym Sci, Part A: Polym Chem Ed 1990;28:1011.
[16] Stone-Masui JH, Stone WEG. Polymer colloids II. New York: Plenum, 1980 (p. 331).
[17] Palit SR, Ghosh PJ. J Polym Sci 1962;58:1225.
[18] Kamel AA, El-Aasser MS, Vanderhoff JW. J Dispersion Sci Technol 1981;2:315.
[19] Cardoso AH, Leite CAP, Galembeck F. Langmuir 1998;14:3187.
[20] Ahmed SM, El-Aasser MS, Micale FJ, Poehlein GW, Vanderhoff JW. Org Coat Plast Chem 1980;43:120.
[21] Newbury DE. Principles of analytical microscopy. New York: Plenum, 1986.
[22] Su LS, Sunil J, Fitch RM. Colloid polymers. London: Academic, 1995.
[23] Smithan JB, Gibson DV, Napper DH. J Colloid Interface Sci 1973;45:211.
[24] Van den Hul HJ, Vanderhoff JW. Br Polym J 1970;2:121.